Microstructure and mechanical properties of Inconel 718 and Inconel 625 produced through the wire + arc additive manufacturing process

William Sean James, Supriyo Ganguly, Goncalo Pardal
Welding Engineering and Laser Processing Centre, Cranfield University
Cranfield, Bedfordshire, MK43 0AL
UNITED KINGDOM

w.james@cranfield.ac.uk

Keywords: Additive manufacture, characterisation, mechanical properties, Inconel 718, Inconel 625

ABSTRACT

In developing the wire + arc additive manufacturing (WAAM) process for heat and creep resistant alloys, structures were built from nickel-based superalloys Inconel 718 (IN718) and Inconel 625 (IN625). In this paper, wall structures were deposited in both superalloys, using a plasma transferred arc process. The microstructure was analysed optically and under SEM; both alloys revealed typical dendritic structure with long columnar grains, with little variation between the alloys. The findings suggest that the structures included significant segregation of alloying elements, with potential intermetallic phases e.g. Laves phases and δ-phases also found across the alloys, which showed significantly more segregation of Nb and Mo at the grain boundaries and inter-dendritic regions. The alloys also underwent room temperature mechanical testing, in addition to this IN625 specimens were tested after a solutionising and ageing treatment. Hardness measurements indicated that in general the WAAM process has the effect of increasing material hardness by approximately 10 %, when compared to wrought alloy in a solutionised state. In IN625 the heat-treated specimens showed an increase in hardness of around 6 %, when compared with its as-deposited condition. Elongation in IN625 showed much greater values. Overall, IN718 showed a greater strength with less elongation than IN625. A comparison between both alloys and their stated maximum UTS and YS values from literature revealed that WAAM built IN718 and IN625 in its as-deposited condition can achieve just over half the maximum achievable UTS, with no post-process treatment. The heat-treatment process tested in IN625 marginally reduced the gap in UTS performance by 3.5 %.

1.0 INTRODUCTION

Wire + Arc Additive Manufacturing (WAAM) has been undergoing development since the 1990's. WAAM is "the combination of an electric arc as heat source and wire as feedstock" (Williams et al., 2016). WAAM is not dissimilar to more traditional manual welding technologies such as TIG/MIG welding (Kou, 2003), with the exception that WAAM uses traditional arc welding technologies with a motion control system, such as a robotic system or retrofitted onto a computer numerical control (CNC) system (Williams et al., 2016). The main difference in automated welding systems and the WAAM system is the thermal profile of as-deposited WAAM components. To build shapes and subsequent components WAAM deposits the wire feedstock in a layer-by-layer manner (Xu et al., 2018a). Unlike other more well established additive manufacturing (AM) methods WAAM is often not used to manufacture a finished product, instead WAAM is used to deposit a net-shape product (Baufeld et al., 2010), which can then be further processed, if required, to achieve a finished product.

As a method to rapid prototype metal structures WAAM is often advantageous over more traditional methods such as machining. As WAAM only deposits the net shape of the product, compared with

machining WAAM is capable of reducing: the waste material, cost, and lead time. (Baufeld et al., 2010).

Superalloys are defined as "a group of nickel-, iron-nickel-, and cobalt-base materials that are used at temperatures of 540 °C and above" (Davis, 1997). Superalloys were initially developed for use in superchargers in aircraft piston engines, however much of their later development was in components for gas-turbines. Nickel-based superalloys can be found in gas-turbines for a variety of applications from aerospace to power generation. Newer gas-turbines operate at higher temperatures than has been seen historically, due to increasing demand for more efficient engines, the nickel superalloys in these environments experience operating temperatures of between 650-700+ °C (Akca and Gürsel, 2015).

The use of WAAM to manufacture components from heat resistant alloys is a relatively new area of study with a relatively low volume of research published in this area. The impact of the WAAM process on the high temperature material properties of heat resistant alloys is largely unknown. Alloys that have been investigated in this study include those suitable for high temperature applications, including largely nickel based super-alloys, this is due to the high temperature performance of these alloys.

Another type of AM process that has been considered as less appropriate for the high-speed flight application include the powder-bed laser AM process. The powder bed process is also a process by which shapes are produced by a layer-by-layer process, however metallic powder particles are used as the feedstock which is then melted to form the part via laser. Benefits that the powder bed AM process shares with the WAAM process includes the ability to produce complex shapes that would be difficult to produce by traditional machining methods (Wang et al., 2017), as well as greater efficiency brought by the minimal waste that is produced by most AM processes. There are, however, some limitations of powder-bed over WAAM which makes WAAM more appropriate for this application. WAAM is more suited to the production of larger scale parts as well as being capable of a higher deposition rate of material. The metallic powder used in powder-bed is more expensive to produce than wire-feedstock, which being coupled with powder loss (which can be as high as 25 % even for more advanced versions of the technology), makes powder-bed produced parts less economical (Tanvir et al., 2020). Larger powder-bed produced components can include pores in the structure which reduces the mechanical performance. In terms of loss of material, WAAM can operate with near to no loss of raw material and can produce pore free structures (Tanvir et al., 2020). After post-processing heat-treatment Wang et al. found that powder-bed produced IN718 was comparable in room temperature tensile strength as the wrought alloy (Wang et al., 2017). For IN625, Tanvir et al. found that WAAM built parts needed further research to achieve the same strength level as powder-bed produced parts, and recommended that a solutionising treatment for IN625 might further increase the performance (Tanvir et al., 2020).

High temperature metals that have been deposited by WAAM at Cranfield University so far include:
Nickel alloys:

- Inconel 625 (Xu, 2018)
- Inconel 718 (Xu, 2018)

Refractory metals:

- Tungsten; WAAM is capable of depositing high purity tungsten and other refractory metals (Marinelli et al., 2019).
- Molybdenum (Martina et al., 2016)
- Tantalum (Martina et al., 2016)
- Ti–6Al–4V (Martina et al., 2012) + other less heat resistant alloys (Welding Engineering and Laser Processing Centre Cranfield University, 2019).

In this paper, research performed towards deposition and wall building of IN625 and IN718 using a plasma transferred arc WAAM process are discussed. A comparison of the two WAAM built alloys was completed and their suitability for high-speed flight applications was discussed.

2.0 MATERIALS AND METHODS

2.1 Overview of Design Parameters

There is interest in developing AM alloys specifically for use as structural components in high-speed missiles with short flight times (< 1 hour). In service temperatures could reach 1000 K for external structural components, or even 1200+ K for components in the propulsion flow path. These components will be highly stressed to minimise structural mass. The desired aim is for the WAAM built alloys to achieve properties similar to currently available wrought materials, such as IN718 (standard) or Haynes 282 (best case), and ideally have low thermal expansion. Creep is not considered to be a major issue due to the short flight time, but there is a lack of data in this regime (high stress, high temperature and short duration). With a focus on very good short-term properties and a particular importance on high temperature performance of these alloys, the room temperature data shown in this paper is a precursor to further high temperature investigations.

2.2 Deposition Process

2.2.1 Inconel 625

IN625 was deposited via a WAAM system consisting of a Kuka six-axis robot, a plasma power source, a water-cooled plasma welding torch mounted to the robot, an external wire feeder, and a part rotator – allowing for symmetrical layer-by-layer WAAM wall building. Also attached to the robot head was a trailing shield (shown in Figure 1) which surrounded the welding torch and extended behind the torch, this provided an argon environment during the WAAM process to prevent excessive oxidisation. The experimental set-up is shown in Figure 2.

The process used for IN625 was a symmetrical wall building process, where two wall structures were built simultaneously on opposite sides of the substrate plate and the part rotator is utilised to alternate between the two sides of the substrate plate. The benefits of this process over a single sided operation is intended to reduce residual stresses on the structure as the warping of the substrate is effectively 'cancelled out' when welded on both sides (Williams et al., 2016). It also has the effect of increasing productivity as inter-pass cooling can partially take place on one side when the process is ongoing on the opposite side, minimising the time the system remains inactive while cooling takes place.

Directly below the trailing shield at a torch-to-work distance of 8 mm, argon shielding was provided to keep the level of oxygen below 800 ppm, with an argon flow of approx. 80 l/min.

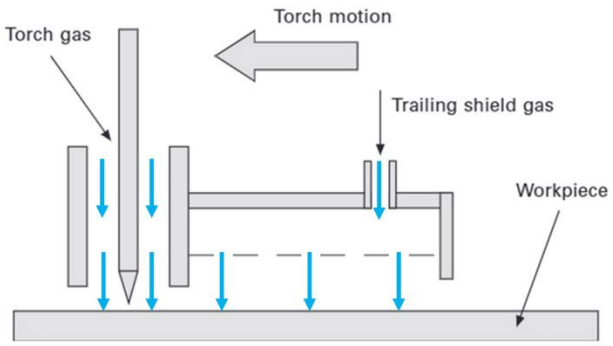

Figure 1: Trailing shield device used during deposition of IN625 (Norrish, 2006), blue arrows

indicate gas flow direction.

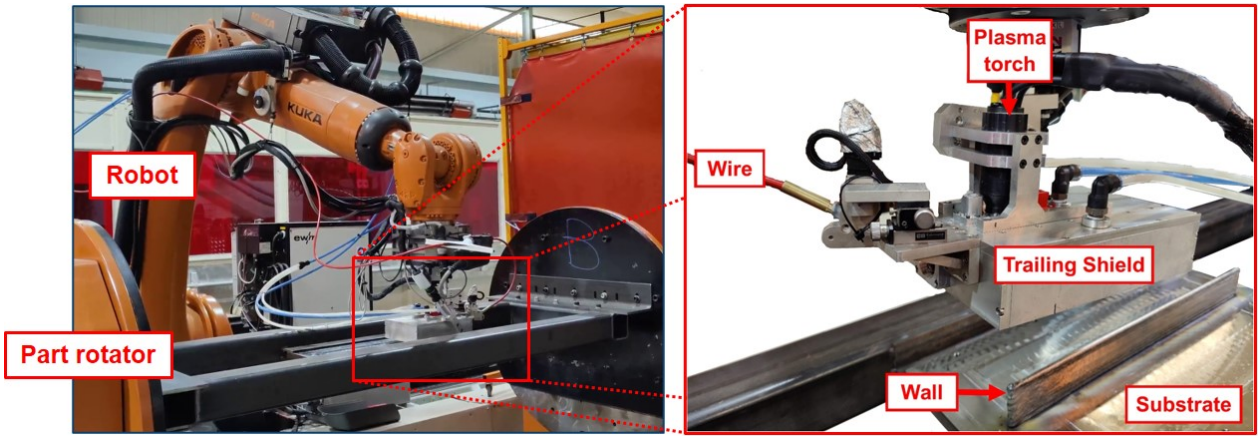

Figure 2: Experimental set-up used to deposit IN625. Boxed area in the LH image is shown in further detail in RH image.

2.2.2 Inconel 718

For the Inconel 718 (IN718) alloy, a WAAM system consisting of three-axis linear CNC system, a Tecarc 320 A AC/DC plasma power source, a water-cooled plasma torch mounted to an adjustable jig on the CNC system, an external wire feeder and a glove box filled with Pureshield argon, controlled below 800 ppm controlled as in section **Error! Reference source not found.**.

The process used for the deposition was a linear wall building system where the layers were deposited in a single direction on a single side of the substrate, due to the limitations of the system used. The experimental set-up used to deposit IN718 is shown in Figure 3.

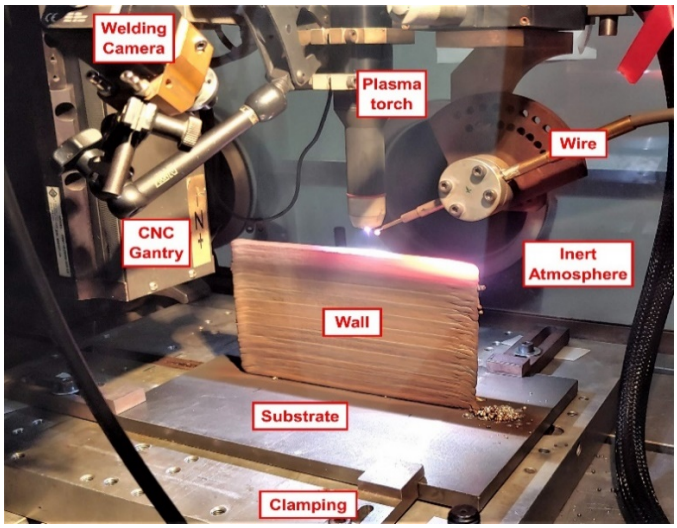

Figure 3: Experimental set-up used to deposit IN718.

2.2.3 Materials

The dimension of the nickel wires used and the welding parameters for each alloy are shown in Table 1 and the chemical composition of these wires is shown in Table 2. For both alloys a 10 mm thick mild steel plate

was used as the substrate. Large linear wall structures were deposited in each alloy measuring approx. 500×110×8 mm for IN625 and 315×110×8 mm for IN718, Figure 4 shows directional axes and orientation of extracted tensile specimens. The welding parameters were kept constant, with the exception of the initial welding layers, where a slower travel speed and reduced wire feed speed were used to better the wetting of the deposit onto the substrate plate.

Table 1: Wire and welding parameters.

	IN718	IN625
Wire Diameter (mm)	1.2	1.2
Torch to work distance (mm)	8	8
Current (A)	180	180
Wire feed speed (m/min)	1.8	2
Travel speed (mm/sec)	5	6
Inter-pass cooling time (min)	3	3

Table 2: Elemental composition of IN718 and IN625 filler wires, %wt. (Elements <0.01% omitted)

	C	Ni	Cr	Mo	Fe	Al	Ti	Nb	Mn	Si	Cu
IN718	0.04	53.57	18.56	2.87	17.8	0.60	0.97	5.01	0.10	0.08	0.07
IN625	0.01	64.75	22.16	8.79	0.24	0.17	0.19	3.60	0.02	0.04	0.02

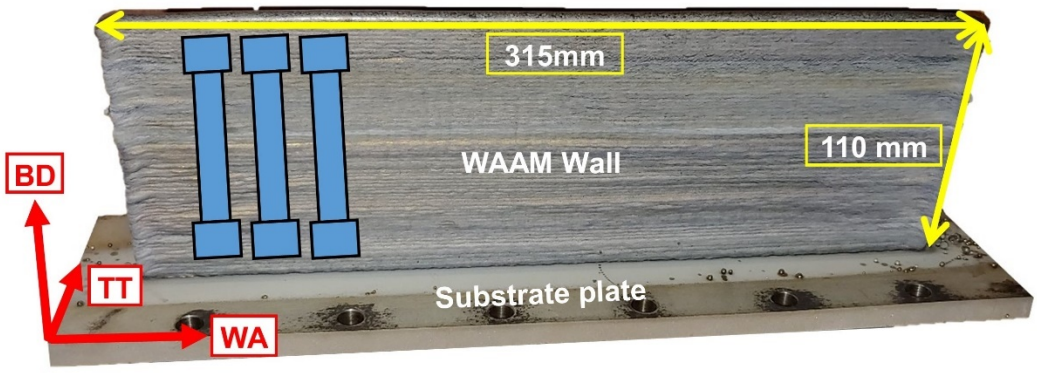

Figure 4 WAAM wall labelled with build dimensions and directional axes. Build direction (BD), through thickness (TT), wall axis (WA).

2.3 Analytical Methods & Mechanical Testing

In IN718 and IN625 alloys, WAAM walls of 226, and 130 layers respectively were built. Once completed the walls were cut from the substrate plates and samples were extracted both along the wall height and length. Cross-sections were extracted and prepared for metallographic analysis following a procedure consisting of mounting, grinding, polishing, and etching. IN718 samples were etched in Kalling's 2 while IN625 was etched in aqua regia. The microhardness was measured using a Zwick/Roell hardness tester under

a load of 500 g and holding time of 15 s, welding filler wire samples of the alloys also underwent a similar process as above to obtain comparative results for the hardening effect of the WAAM process. The microstructure was also analysed, using a Tescan VEGA 3 scanning electron microscope, and optically using a Leica DM 2700M Microscope. To determine composition an Oxford Instruments X-Max 20 mm was used in combination with the SEM for the EDS analyses.

For room temperature mechanical testing an Instron 5500R Electro-mechanical testing machine was used with a load cell of 100 kN and a crosshead speed of 1 mm/min. Elongation was measured using a laser extensometer over a gauge length of 25 mm. At least three samples were tested for each condition (orientation, as-deposited and heat-treated variants), and samples conformed to ASTM E8/E8M subsize specimen standard. A schematic drawing of the tensile specimens used is shown in Figure 5.

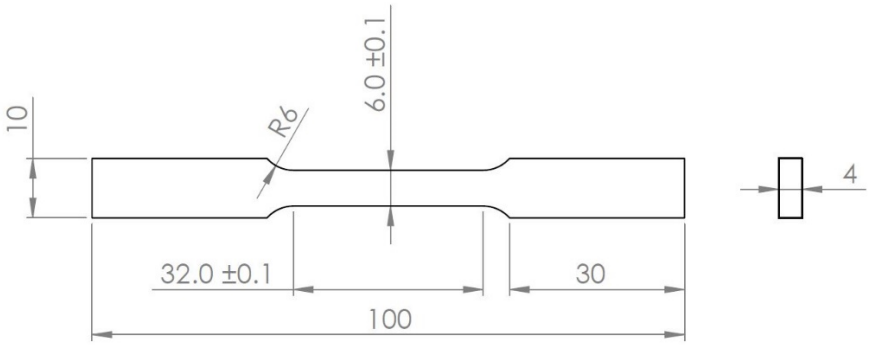

Figure 5: Dimensions (in mm) of the tensile specimens used for RT tensile testing, conforming to ASTM E8/E8M subsize standard.

2.3.1 Post-process Treatment of Inconel 625

A heat-treatment was conducted on several IN625 tensile specimens. The heat treatment made use of a Carbolite Gero CWF 11/13 furnace and consisted of a two-stage heating process, a solutionising and heat-treating process. The first stage included heating the samples in the furnace to 1100 °C holding at this temperature for 15 mins, with the aim to dissolve Laves and secondary phases. After this process the specimens were water quenched to room temperature. The specimens then underwent an ageing process at 750 °C for 8 hours, followed by air cooling to room temperature. The aim of the second stage was to increase the mechanical strength through the precipitation of γ″ Ni_3Nb in the inter-dendritic regions (Kasravi et al., 2021). This treatment was used in a previous study on IN625 by Cortial et al (Cortial et al., 1995).

3.0 RESULTS

3.1 Macrostructure

The macrostructure seen in the samples of the as-deposited IN718 WAAM wall, i.e. without any additional heat or solution treatment to the material are shown in Figure 6 with an enlarged image at higher magnification shown in Figure 7. In the macrostructure large cracks can be seen extending through the layers. IN718 exhibits a typical solidified dendritic structure made up of large columnar grains which appear to extend along the height of the wall in the build direction (BD seen in Figure 6), this structure was expected and has been seen in previous studies namely by Xu et al (Xu et al., 2018b).

IN625 exhibits a similar structure to IN718 as can be seen in Figure 8. Nearest the substrate in both alloys, it can be seen that the structure has much finer cellular grains, whereas in later layers extending though the

build direction grains get steadily longer exhibiting a more columnar dendritic structure. Overall, more cracking was seen in IN718.

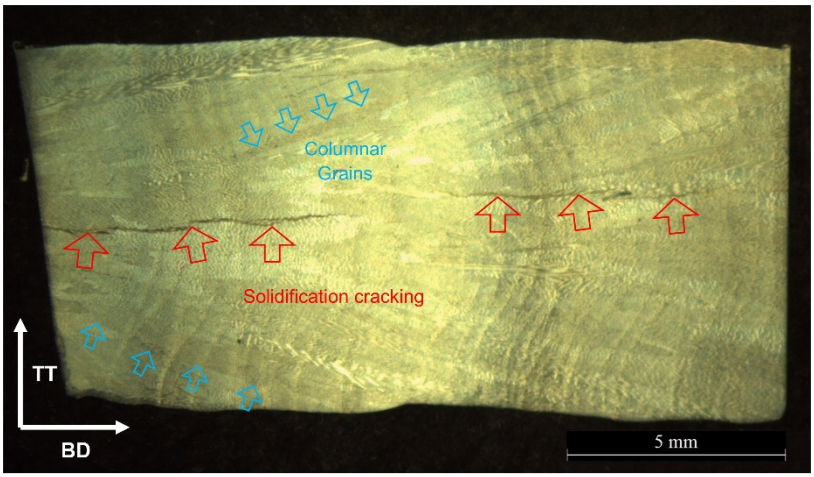

Figure 6: Macrograph cross-section of as-deposited IN718. This is a sample near to the top of the wall. From bottom to top of the build direction is shown from left to right. Red arrows indicating solidification cracking, blue arrows show columar grains.

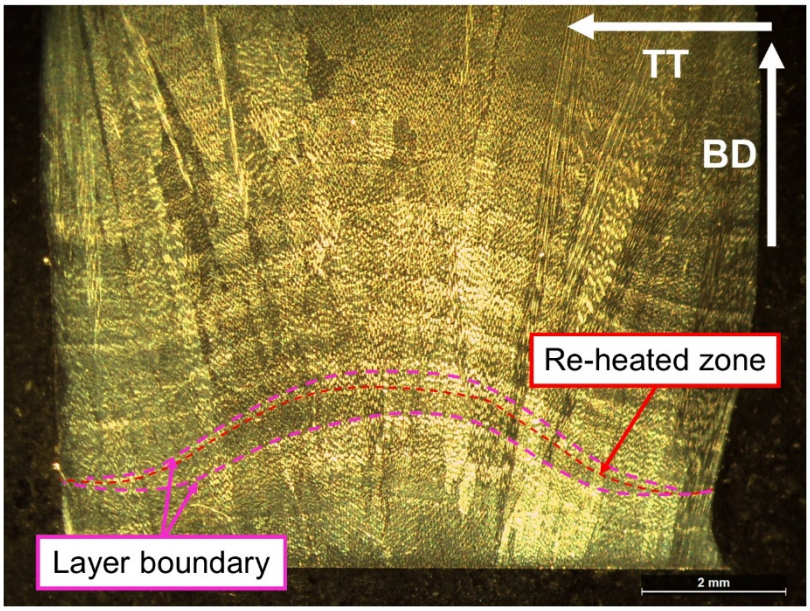

Figure 7: Macrograph cross-section of as-deposited IN718, showing layer boundary and re-heated zone Pink dotted line and arrows showing boundary between layers and red dotted line shows re-heated zone.

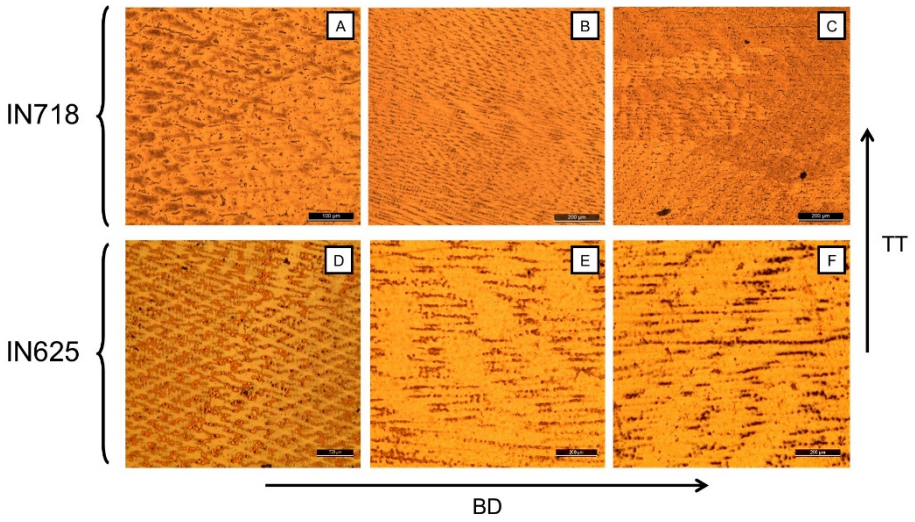

Figure 8: Optical micrograph of as-deposited macrostructure of IN718 and IN625 samples. Top three images show IN718, bottom three images show IN625.

3.2 Microstructure

The microstructure seen in IN718 at the grain boundary is shown in Figure 9. The as-deposited WAAM structure shows significant amounts of segregation of Nb and Mo at the grain boundaries, an EDS analysis of the area revealed the lighter coloured phases to be Ni_2Nb (green arrows), purely based on the similarity in the composition and closeness to the atomic percentages of the A_2B type Ni_2Nb Laves phase seen in literature (Xu et al., 2018b). This phase can also clearly be seen on the elemental map (Figure 10), which shows the segregation of Nb as well as the depletion of heavier metals such as Nb and Mo in the surrounding regions.

The red arrows in Figure 9 are indicating Ti rich phases, which appears as smaller darker precipitates. These precipitates have been identified as a possible MC type carbide TiC based on appearance seen in literature and composition of approximately 50 % Ti (Mitchell, 2010).

An analysis into the composition of the above precipitates seen in IN718 was carried out, the composition is shown in Table 3. The composition of area B, highlighted in yellow in Figure 9, shows a significant increase over base values of Nb while the amount of Ni has decreased significantly. Comparing the values in terms of atomic percentage, suggests that the composition is very close to that of Ni_2Nb. While area D shows a significant increase in both Ti, Nb and Al without any indicated elements.

The solidification cracks seen in IN718 were also analysed based on composition and found to contain Ni_2Nb Laves phase at the crack edge, as seen in Figure 11 the lighter coloured phases along the crack also form the root of the crack.

The microstructure of heat-treated IN625 is shown in Figure 12, although this image is not of a grain boundary location, the phases seen appear smaller and more evenly distributed. The purpose of the post-deposition heat-treatment was to dissolve Laves phase and allow for the formation of more useful γ'' strengthening phase. It does appear that a significant amount of potential Laves phases have been dissolved compared to as-deposited IN718, although some that remains are similar in appearance however smaller in size than was seen in IN718. In IN625 the darker Ti rich zones (shown as area F in Figure 12, with composition in Table 3) also appear and typically vary in size and are seen at a greater frequency than those seen in IN718.

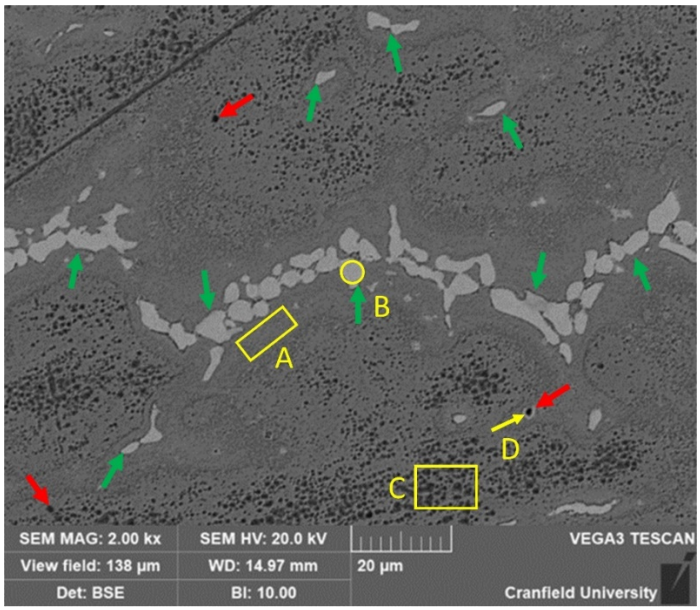

Figure 9: Microstructure in IN718 showing grain boundary and segregated zones, in the through thickness (TT) and wall axis (WA) cross-section. This sample is located mid-height in the build direction. Green arrows showing lighter coloured segregated Ni2Nb, red arrows indicating Ti rich carbides. In yellow are areas where the composition was analysed (Table 3).

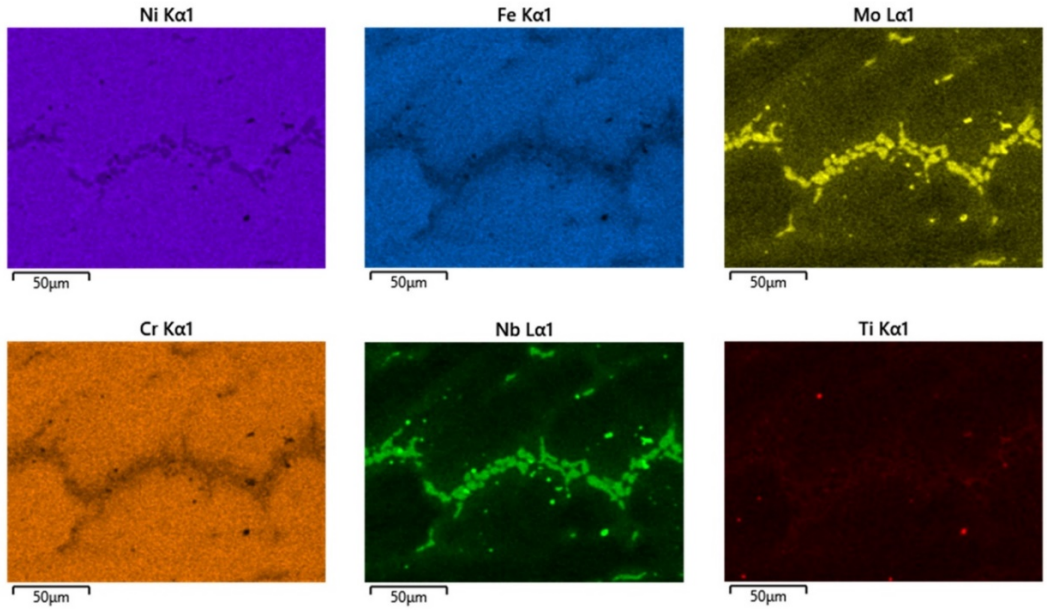

Figure 10: EDS Elemental map of IN718 segregated zone.

Table 3: EDS composition of alloys, labelled A – D on IN718 SEM image (Figure 9), E – F on IN625 SEM image (Figure 12). Values proceeded by a green (+) represent a significant increase over base values, values with a red (–) represent significantly less and a purple (*) represent anomalous elements.

Spectrum Label	% At.						
	IN718				IN625		
	A	B	C	D	E	F	G
C	(+)12.04	(–)0	(+)10.02	(–)0	(+)18.35	(+)12.82	(+)9.73
F	(*)6.95						
Al	1.11	(–)0	1.25	(+)15.20	(–)0.22	0.31	0.38
Si					(*)0.73	(*)0.18	(*)0.12
Ti	1.50	1.95	0.63	(+)51.85	0.25	(+)1.52	0.17
Cr	16.64	(–)17.67	19.97	(–)0	(–)17.24	20.32	23.64
Fe	13.77	(–)12.96	18.30	(–)0		(–)0.17	(–)0.21
Ni	42.51	(–)46.26	46.92	(–)0	(–)35.18	(–)50.61	60.36
Nb	3.91	(+)21.15	(–)1.39	(+)32.95	(+)16.46	(+)7.81	(–)1.00
Mo	1.58	(–)0	1.53	(–)0	(+)11.58	6.25	4.39

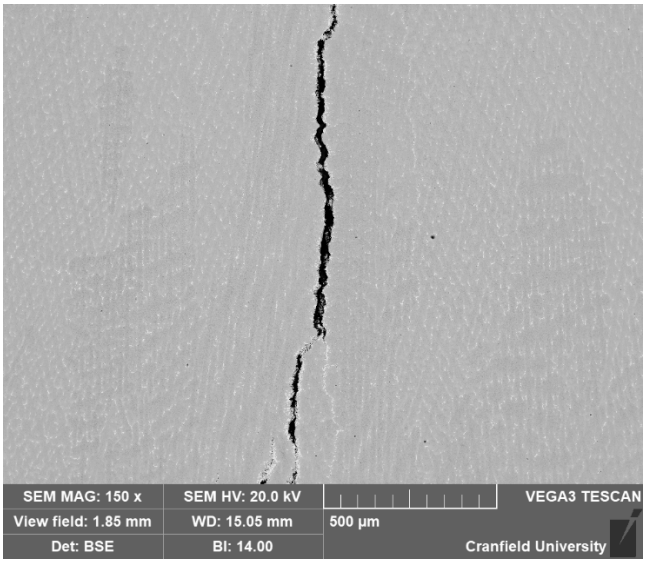

Figure 11: Solidification crack seen in IN718, showing lighter coloured Laves phases in crack root. Through thickness (TT) and build direction (BD) cross-section.

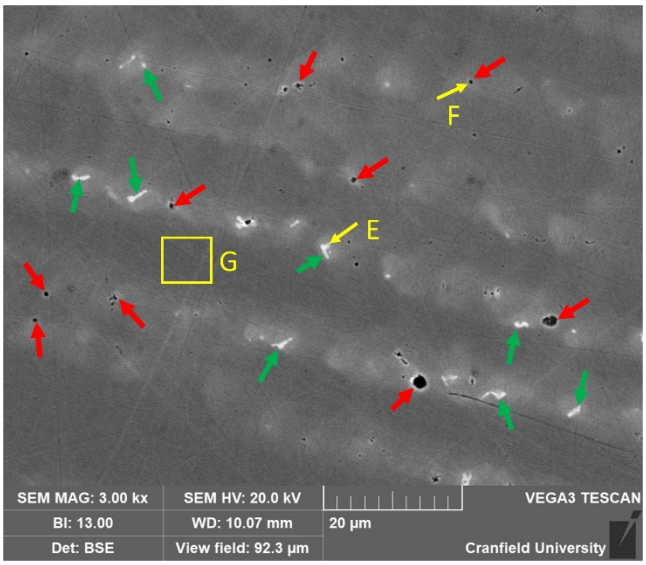

Figure 12: Microstructure of post-deposition heat-treated IN625 showing segregated zones, in the through thickness (TT) and wall axis (WA) cross-section. This sample is located mid-height in the build direction. Green arrows showing lighter coloured segregated Ni2Nb, red arrows indicating Ti rich zones possible Ti rich carbides. In yellow are areas where the composition was analysed (Error! Reference source not found.**).**

3.3 Hardness Comparison

Hardness between both alloys, in their as-deposited condition was compared. As-deposited IN625 was also compared with its heat-treated variant. The hardness was tested at 1 mm increments along the surface of the samples. Micro hardness results were obtained using a Zwick/Roell hardness tester under a load of 500 g and holding time of 15 s, results are displayed as Vickers Hardness in Table 4. A comparison of the data revealed that IN718 is harder than IN625, with average values for both alloys at 293.9 HV and 248.5 HV respectively. The heat-treatment that IN625 underwent showed a marginal increase in the average micro hardness with a value of 262.75 HV, representing a 5.7 % increase over the as-deposited average.

Table 4: Vickers hardness values. [a](Xu et al., 2018b), [b](Special Metals, 2007), [c] (Kasravi et al., 2021), [d] (Special Metals, 2013)

Alloy	Condition		Hardness (HV)
IN718	WAAM	as-dep	293.9
		Heat treated	388 [a]
	Wrought		354 [b]
IN625	WAAM	as-dep	248.5 [c]
		Heat treated	262.8 [c]
	Wrought		238 [d]

3.4 Room Temperature Tensile Comparison of Inconel 718 & 625

Room temperature tensile test comparison between as-deposited IN718 and IN625 revealed that IN718 had an average UTS of 841.7 MPa compared with an average of 622.2 MPa for IN625. YS for both IN718 and

IN625 was calculated to be 528.8 MPa and 396.7 MPa respectively. Elongation on average was substantially higher in IN625 than was seen in IN718, with the IN625 specimens breaking on average at +57 % of their original length and IN718 specimens breaking at an average of +30.5 % of their original length. Overall IN718 showed greater strength with less elongation than IN625. The alloys were then compared against their stated maximum UTS and YS values from literature, which revealed that WAAM built IN718 and IN625 in its as-deposited condition can achieve approximately 62 % of the maximum achievable UTS (64.5 % for IN625, 58.7 % for IN718), with no post-process treatment. With heat-treatment however, IN625 was able to reduce the gap slightly in UTS performance compared to literature to 68 % of maximum performance. Heat treated IN625 also resulted in a reduction in elongation compared with as-deposited material, bringing it below the value given for the wrought alloy. Tensile testing results compared with wrought alloy are shown in Table 5. A stress/strain graph of the best and worst performing sample in each category is shown in Figure 13, where the suffix (A) is the best performance and (B) the worst. As IN718 is more age-hardenable than IN625, IN718 did not undergo a heat-treatment. A comparison between the alloys in their partially aged (as-dep) condition is more prudent.

Table 5: Mechanical tensile testing results for IN718 and IN625, with wrought data (Donachie, 2002).

Alloy	Condition		UTS (MPa)	0.2 % YS (MPa)	Elongation (%)
IN718	WAAM	as-dep	841.70	528.84	30.47%
	Wrought		1435	1185	21%
IN625	WAAM	as-dep	622.21	396.67	57.26%
		Heat treated	659.70	328.36	41.88%
	Wrought		965	490	50%

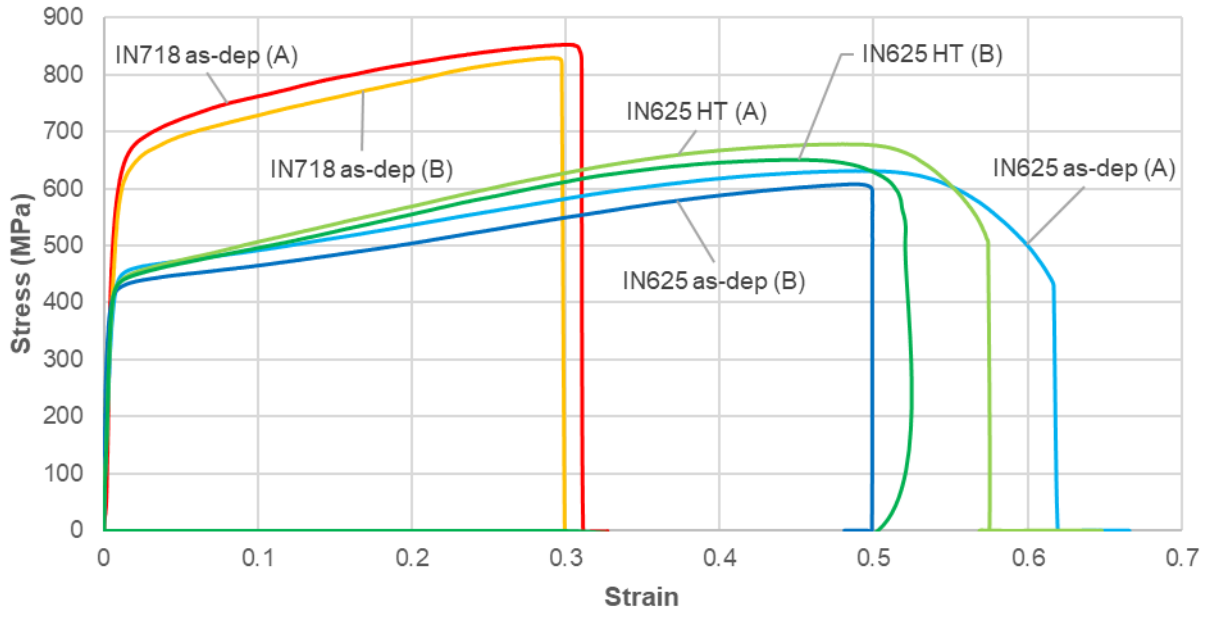

Figure 13: RT Stress vs. Strain for as-deposited IN718, IN625 & Heat-treated (HT) IN625. Best (A) and worst (B) performing samples are shown in each category.

4.0 DISCUSSION

4.1 Macro and Microstructure

The macrostructure of both alloys are very similar in appearance, and exhibit the same characteristics in relation to the earlier and later built layers as shown in Figure 8. In IN718 much more cracking was observed compared to IN625, it is possible that the different building process is the cause with slightly different equipment and parameters used to deposit the alloys, even though conditions inside the enclosure should have been more optimum for oxidisation induced cracks. It is also possible that as IN625 was built in a more open environment and onto larger equipment that the rate of cooling for IN625 was faster than IN718, meaning IN718 was effectively aged more as part of its WAAM process than IN625 experienced. The data for hardness would also suggest that IN718 was harder in its as deposited condition that IN625 which could suggest that IN718 was more brittle and hence more prone to cracking, this would also explain the large difference between the elongation of the alloys during tensile testing, with IN718 relativity restrained compared with IN625.

The columnar grains (seen to grow through the layers and across the height of the walls in both alloys), are similar to what has been seen in previous studies on as-deposited material, where the columnar dendrites are not precisely vertical but extend at an angle of approx. 70 ° to the substrate. This was also seen in a study by Wang et al, in which the reason for this was related to heat flux direction, where dendrite growth follows the maximum temperature gradient, which is opposite to the unidirectional heat flux direction (Wang et al., 2016).

The potential Ni_2Nb Laves phase seen at the edge of the crack in Figure 11 suggest that the heavier metals in the alloy, such as Nb, which has a higher melting point than the other elements, are segregating from the rest of alloy during solidification. The root of the cracks also appears to be filled with the same compound suggesting that the formation of these Laves phase are the cause of the cracking seen in the alloy. The size however of the columnar grains seen, especially in the as-deposited material, of both alloys may suggest that there is in fact less grain boundary area for these precipitates to form and consequently they have less of a reducing effect on the strength.

Laves phase formation in alloys are known to be detrimental to the performance as it depletes the elements that would otherwise form more useful substances such as precipitation hardening carbides (Donachie, 2002), or strengthening phases. The solution treatment that IN625 underwent was performed to homogenise the microstructure and by dissolving Laves phases into the matrix which could then form the γ″ strengthening phase, which is shown under SEM to have reduced the size and frequency of Laves phases. Generally, the results from the SEM and EDS analysis of the microstructure give a good indication of the presence of the Laves phases described, such as Ni_2Nb in IN625 and IN718. For example, looking at Table 3 a simple calculation of multiplying the value for Nb by two to get a rough value for Ni, seems to confirm the presence of Ni_2Nb for both spectrum B and E within 2-4 % At.

However, further work to confirm the presence of Laves phases would help to eliminate any doubt that remains. Another point for further investigation is the appearance of Ti rich zones in both alloys, but specifically the appearance of the Ti rich zones in IN625 which appeared in a greater frequency in heat-treated IN625 than those seen in as-dep IN718 despite the matrix containing significantly less Ti than IN718.

The heat treatment process that IN625 underwent which was based on a previous study on the alloy by Cortial et al. In the study, Cortial et al found that the treatment resulted in increased mechanical strength due to the precipitation of γ″ Ni_3Nb phase in the inter-dendritic spaces, which is a strengthening phase in IN625 (Cortial et al., 1995). Longer aging time tends to provide a more uniform distribution of these precipitates. γ″ Ni_3Nb and aging of IN625 produces a more carbides in the alloy. Carbides that have been observed in a study by Shaikh et al included carbides rich in Ti, Nb and Si (Shaikh et al., 2000). The fact that Ti rich

carbides have been observed in the literature in the IN625, suggests that the Ti rich zones that exist in the alloys with no other significant increase are Ti carbide. The potential Ti carbides found in IN625 and IN718 were observed to be smaller in size, dark in colour as well as more sparsely distributed, compared to potential Laves phases. Area D of Figure 9 suggest with the significant increase in the percentage of Nb, Ti and Al (over the base values), without the presence of the other elements, that perhaps this is indicative of a complexed carbide where any Carbon has been removed by the etching process, although the presence of Carbon in EDM results is often unreliable.

4.2 Mechanical Properties

The increase in material hardness of IN625 in the as-deposited condition suggests that the cyclic heating of the WAAM process has at least a partial ageing effect on the alloy. This was also seen when IN625 underwent a post-process aging treatment which resulted in an approximate 5.7 % increase in hardness vs. as-deposited material. In the case IN718, the as-deposited hardness was shown to be significantly less than manufacturer's data for the wrought alloy. This is probably due to the more extensive ageing process that IN718 typically undergoes to achieve the best mechanical properties, with proper aging treatment it is anticipated that hardness would further increase. In a study on heat treating WAAM built IN718 Xu et al. found that heat treated material showed an increase in hardness of 158 HV compared with as-deposited material. This represents an approx. 69 % increase (Xu et al., 2018b), highlighting the difference between the aging processes of the two alloys and why a comparison between the aged material is less useful than a comparison between the partially aged as-deposited material.

Overall, the improvement in performance by heat-treating IN625 specimens was disappointing, with only a marginal increase in UTS performance compared to the wrought values given by Donachie in the Superalloys technical guide (Donachie, 2002); which provided data in suitably comparable format. WAAM built IN625 and IN718 has some improvements to be made before it can achieve the performance of the wrought alloys. Xu et al in a paper based on IN718 found that interpass rolling was able to increase the UTS performance of the WAAM built material up to and above what was achievable in wrought alloy, and meet the wrought standard for YS and elongation (Xu et al., 2018b).

In evaluating these two WAAM built alloys for a high-speed flight application, IN718 and IN625 show promise, however further work is required to understand their high temperature performance at a temperature range of RT to 1000 °C, and what effect the heat-treatment process will have on the performance at elevated temperatures. An investigation into the interpass rolling process described by Xu et al would also be desirable to understand the performance of the rolled WAAM alloys. Finally, IN718 at least at RT would appear to be preferable over IN625 for its higher strength performance, however IN718 does appear to be a harder more brittle alloy and the results of the RT study do correlate to what the data suggested for the wrought alloys. Further study into the high temperature performance of both these WAAM built alloys will help to understand their performance for high-speed flight.

5.0 CONCLUSIONS

1. WAAM built material of IN718 at room temperature had a higher UTS and YS performance, however IN625 had a much greater elongation under testing. Perhaps, although a high frequency of Nb rich segregated compounds were found along the grain boundary in IN718, the larger columnar grains provided less grain boundary area for the precipitation of segregated compounds to form. This difference may also be due to IN718 potentially being partially aged to a larger extent during the deposition process than IN625.

2. A heat-treatment consisting of solutionising and heat-treatment had the effect of increasing the performance of IN625 by approx. 6 %, which was less than anticipated but may have been due to

cracking seen in the alloy which potentially reduced its performance.

3. Refractory elements Nb, Mo segregate and contribute to formation of Laves phases, specifically Ni_2Nb, which were indicated in both alloys with precipitation seen at the grain boundaries and interdendritic regions.

4. The heat treatment process was found to increase hardness of IN625 by an average of 5.7 % compared with as-deposited WAAM material, and when compared with manufacturer's data on the wrought alloy an increase of 10.4 %.

ACKNOWLEDGEMENTS

The authors wish to acknowledge the UK Ministry of Defence for their financial support, and the industrial supervisors from DSTL Porton Down, for their ongoing advice and guidance: Mr Graham Simpson, Dr Sarah Baker and Dr Matthew Lunt.

The authors would also like to acknowledge the expert help from welding technicians Mr Flemming Nielsen, Mr Nisar Shah, and Lab manager Mr John Thrower, without whom this work would not have been possible. The technical assistance of Mr Steve Pope and Mr Kristopher Bramley for their help with imaging during the Coronavirus lockdowns. As well as the Cranfield MSc students whose group project contributed to the experimental data presented in this paper.

REFERENCES

Akca, E., Gürsel, A., 2015. A Review on Superalloys and IN718 Nickel-Based INCONEL Superalloy. Period. Eng. Nat. Sci. 3. https://doi.org/10.21533/pen.v3i1.43

Baufeld, B., Biest, O. Van der, Gault, R., 2010. Additive manufacturing of Ti-6Al-4V components by shaped metal deposition: Microstructure and mechanical properties. Mater. Des. 31, S106–S111. https://doi.org/10.1016/j.matdes.2009.11.032

Cortial, F., Corrieu, J.M., Vernot-Loier, C., 1995. Influence of heat treatments on microstructure, mechanical properties, and corrosion resistance of weld alloy 625. Metall. Mater. Trans. A 26, 1273–1286. https://doi.org/10.1007/BF02670621

Davis, J.R., 1997. ASM Specialty Handbook: Heat-Resistant Materials, in: ASM Specialty Handbook: Heat-Resistant Materials, ASM Specialty Handbook. ASM International, p. 36.

Donachie, M.J., 2002. Superalloys: A Technical Guide, 2nd Edition. America (NY). https://doi.org/10.1361

Kasravi, N., Hidayat, R., Tuncer, C., Themistokleous, M., Sambo, A.M., 2021. Additive manufacture of alloys for high temperature application. Cranfield University.

Kou, S., 2003. Welding Metallurgy, 2nd ed. ed. Hoboken, N.J. : Wiley-Interscience.

Marinelli, G., Martina, F., Ganguly, S., Williams, S., 2019. Development of Wire + Arc additive manufacture for the production of large-scale unalloyed tungsten components. Int. J. Refract. Met. Hard Mater. 82, 329–335. https://doi.org/10.1016/j.ijrmhm.2019.05.009

Martina, F., Marinelli, G., Ganguly, S., Williams, S.W., 2016. Wire + Arc Additive Manufacturing of

Refractory Metals.

Martina, F., Mehnen, J., Williams, S.W., Colegrove, P., Wang, F., 2012. Investigation of the benefits of plasma deposition for the additive layer manufacture of Ti-6Al-4V. J. Mater. Process. Technol. 212, 1377–1386. https://doi.org/10.1016/j.jmatprotec.2012.02.002

Mitchell, A., 2010. Primary Carbides in Alloy 718, in: 7th International Symposium on Superalloy 718 and Derivatives 2010. The Minerals, Metals & Materials Society, pp. 161–167.

Norrish, J., 2006. Advanced welding processes : technologies and process control, [New editi. ed.

Shaikh, M.A., Ahmad, M., Shoaib, K.A., Akhter, J.I., Iqbal, M., 2000. Precipitation hardening in Inconel 625. Mater. Sci. Technol. 16, 129–132. https://doi.org/10.1179/026708300101507613

Special Metals, 2013. INCONEL® alloy 625 [WWW Document]. URL https://www.specialmetals.com/assets/smc/documents/alloys/inconel/inconel-alloy-625.pdf (accessed 6.4.20).

Special Metals, 2007. INCONEL® alloy 718 [WWW Document]. URL https://www.specialmetals.com/assets/smc/documents/inconel_alloy_718.pdf (accessed 5.8.20).

Tanvir, A.N.M., Ahsan, M.R.U., Seo, G., Kim, J. duk, Ji, C., Bates, B., Lee, Y., Kim, D.B., 2020. Heat treatment effects on Inconel 625 components fabricated by wire + arc additively manufacturing (WAAM)—part 2: mechanical properties. Int. J. Adv. Manuf. Technol. 110, 1709–1721. https://doi.org/10.1007/s00170-020-05980-w

Wang, J.F., Sun, Q.J., Wang, H., Liu, J.P., Feng, J.C., 2016. Effect of location on microstructure and mechanical properties of additive layer manufactured Inconel 625 using gas tungsten arc welding. Mater. Sci. Eng. A 676, 395–405. https://doi.org/10.1016/j.msea.2016.09.015

Wang, X., Gong, X., Chou, K., 2017. Review on powder-bed laser additive manufacturing of Inconel 718 parts. Proc. Inst. Mech. Eng. Part B J. Eng. Manuf. 231, 1890–1903. https://doi.org/10.1177/0954405415619883

Welding Engineering and Laser Processing Centre Cranfield University, 2019. MATERIALS AND PROPERTIES [WWW Document]. URL https://waammat.com/about/materials-and-properties (accessed 11.8.19).

Williams, S.W., Martina, F., Addison, A.C., Ding, J., Pardal, G., Colegrove, P., 2016. Wire + Arc additive manufacturing. Mater. Sci. Technol. (United Kingdom) 32, 641–647. https://doi.org/10.1179/1743284715Y.0000000073

Xu, X., 2018. Wire + Arc Additive Manufacture of New and Multiple Materials. Cranfield University.

Xu, X., Ganguly, S., Ding, J., Guo, S., Williams, S., Martina, F., 2018a. Microstructural evolution and mechanical properties of maraging steel produced by wire + arc additive manufacture process. Mater. Charact. 143, 152–162. https://doi.org/10.1016/j.matchar.2017.12.002

Xu, X., Ganguly, S., Ding, J., Seow, C.E., Williams, S., 2018b. Enhancing mechanical properties of wire + arc additively manufactured INCONEL 718 superalloy through in-process thermomechanical processing. Mater. Des. 160, 1042–1051. https://doi.org/10.1016/j.matdes.2018.10.038